John Gaskins
Graduate Research Assistant
Mechanical and Aerospace Engineering,
University of Virginia,
Charlottesville, VA 22904
e-mail: jtg2e@virginia.edu

N. Scott Barker
Professor
Electrical and Computer Engineering,
University of Virginia,
Charlottesville, VA 22904
e-mail: nsb6t@virginia.edu

Matthew R. Begley[1]
Professor
Mem. ASME
Mechanical Engineering Department,
Materials Department,
University of California,
Santa Barbara, CA 93106
e-mail: begley@engr.ucsb.edu

Comprehensive Solutions for the Response of Freestanding Beams With Tensile Residual Stress Subject to Point-Loading

This paper provides comprehensive solutions for the load-deflection response of an elastic beam with tensile residual stresses subjected to point-loading. A highly accurate explicit approximation is derived from the exact implicit solution for moderate rotations, which greatly facilitates property extraction and the design of devices for materials characterization, actuation, and sensing. The approximation has less than 6% error across the entire range of loads, displacements, geometry, and residual stress levels. An illustration of the application of the theory is provided for microfabricated nickel beams. The explicit form provides straightforward estimates for the critical loads and deflection defining the limits where classical asymptotic limits (e.g., pretensioned membrane, plate, and nonlinear membrane) will be accurate. Regimes maps are presented that identify critical loads, displacements, and properties correspond to these behaviors. Finally, the explicit form also enables straightforward estimations of bending strains relative to stretching, which is useful in the design of materials experiments that can be approximated as uniform straining of the beams. [DOI: 10.1115/1.4024785]

1 Introduction

An effective way to measure material properties for thin films is to measure the load-deflection relationship of a freestanding structure, such as a thin beam or wire (e.g., membranes [1–4], microbeams [5,6] and wires [7,8]). Such methods are increasingly popular because a wide range of loads and displacements can be accessed using existing off-the-shelf systems, such as atomic force microscopes (AFM) [7–13], nanoindentation systems, profilometers, and instrumented microindenters [1–6,14,15]. Further, the preparation of specimens amenable to one-dimensional modeling (i.e., beams and wires) is increasingly straightforward with emerging micro- and nanofabrication techniques [16,17]. Arguably the simplest and most accurate method to determine properties using this approach is to choose a combination of loads, displacements, and specimen geometry such that closed-form analytical expressions for load-deflection curves are accurate.

There are several classical limits regarding the mechanical response of beams with explicit analytical solutions, each corresponding to different combinations of applied loads, modulus, and residual stress in the beam [18]. The challenge is to identify the combination of properties that corresponds to each limit, such that an appropriate solution is used to extract properties. For example, linear load-deflection relationships can result from either bending dominated behavior (small values of residual stress and small displacements) or from stretch dominated behavior (i.e., large values of residual stress). Nonlinear load-deflection relationships can be obtained for scenarios where deflections are large, but the threshold of "large" displacements naturally depends on the level of prestretch and so forth. Each of these limits is of interest, as each enables straightforward extraction of various material properties; for example, linear response is useful to extract elastic modulus and residual stress, while large deflections (in which bending is negligible) can facilitate the measurement of nonlinear material response by ensuring uniform stretching in the beam.

Further, the ability to identify various regimes of response is critical to the accurate design of actuators and sensors, such that the appropriate input/output relationships are used. Simply put, given a range of expected properties or desired performance, what dimensions should be chosen in conjunction with a specific instrumentation system (be it for measurement, sensing, or actuation) to ensure the accuracy of analytical solutions? For example, one might like to know the combination of deflections and beam sizes that can be chosen to ensure that bending strains are negligible, such that the test can be modeled assuming pure stretching of the beam. These considerations are increasingly important as researchers attempt to decrease the dimensions of test structures down to the nanometer scale [7,8].

In this work, we examine the full nonlinear load-deflection response of elastic beams with tensile residual stress and identify the relevant asymptotic limits corresponding to classical types of response. Design maps are constructed to illustrate critical values of load and displacement that identify regimes where these limits are accurate, using dimensionless parameters involving prestretch, modulus, and dimensions. These maps can be used to identify appropriate geometries, loads, and deflections to target modulus and/or residual stress. Further, we identify a simple closed-form expression for nonlinear responses that facilitate property extraction when asymptotic expressions are not valid. A critical contribution is the development of an *explicit* analytical relationship for load-deflection response that avoids the complication of using implicit solutions, which requires nonlinear root-finding to determine the mechanical stretch in the beam.

There are a host of previous experimental studies and theoretical frameworks that utilize some aspects of the results presented here [1,5–10,12,13,19–21]. The current work is a more comprehensive treatment of the response of point-loaded beams in the following respects. First, it includes an analysis that accounts for all levels of residual strain, across the full range of loads and displacements for moderate rotations. Second, it clearly identifies critical loads (or displacements) that define the asymptotic limits where classical solutions are accurate. Third, it provides an accurate explicit approximation for the transition region between various classical limits, which allows for decoupling of the

[1]Corresponding author.
Manuscript received April 2, 2013; final manuscript received June 6, 2013; accepted manuscript posted June 11, 2013; published online September 18, 2013. Assoc. Editor: Chad M. Landis.

contribution of Young's modulus and residual stress. This avoids the need for numerical modeling. Fourth, this work identifies critical loads (or deflections) that define scenarios where bending strains can be ignored and the beam experiences uniform stretching. This contribution will facilitate the design of experiments intended to measure nonlinear (e.g., elastic-plastic) properties, in which the goal is to utilize a simple analysis of stretching with nonlinear material response. Finally, the approximate solution is used to decouple modulus and prestrain for experimental tests on thin film nickel beams. The results are consistent with those found in literature and, thus, demonstrate the effectiveness of the solutions in analyzing the properties of microfabricated beams with submicron thickness.

2 Full Solution and an Effective Approximation

Consider a beam of length L, clamped at both ends and loaded at its center with the point force P. Assuming plane sections remain plane and that the beam is slender enough to ignore transverse shear, and allowing for moderate rotations, the total axial strain in the beam is given by

$$\varepsilon(x) = u'(x) + \frac{1}{2}[w'(x)]^2 - w''(x)\cdot y \tag{1}$$

where y is the distance from the centerline, $u(x)$ is the axial displacement in the beam, and $w(x)$ is the transverse displacement. Let ε_R be a positive prestretch in the beam; that is, ε_R is the mechanical strain in the beam at zero elongation, caused by tensile residual stress created during fabrication. Assuming plane stress[2], the principle of virtual work yields the condition that

$$u'(x) + \frac{1}{2}[w'(x)]^2 + \varepsilon_R = \text{constant} = \lambda^2 \tag{2}$$

where λ^2 represents the spatially uniform mechanical strain in the deformed state (i.e., that associated with the state created by applying the point load) along the neutral axis. Hence, λ also represents the average stress via $\sigma = E\lambda^2$. With this in mind, governing equations that dictate the transverse displacement and mechanical strain in the beam are given by

$$\bar{w}''''(\bar{x}) - \Lambda\bar{w}''(\bar{x}) = 0; \quad \Lambda^2 - \bar{\varepsilon}_R - 12\int_0^{1/2}[\bar{w}'(\bar{x})]^2 d\bar{x} = 0 \tag{3}$$

where $w = h\bar{w}$, $x = L\bar{x}$, $\Lambda = \sqrt{12}\lambda L/h$, and $\bar{\varepsilon}_R = 12L^2\varepsilon_R/h^2$. (These results are for a rectangular beam cross section, although analogous results can be easily obtained for circular beams or wires using suitable normalizations for λ and ε_R.) The boundary conditions are given by

$$\bar{w}(0) = \bar{w}'(0) = \bar{w}'\left(\frac{1}{2}\right) = 0; \quad \bar{w}'''\left(\frac{1}{2}\right) = 96\bar{P} \tag{4}$$

where $\bar{P} = P/P_o$, with $P_o = 16Ebh^4/L^3$ representing the applied load (P_o) at which the center-point deflection will equal the beam thickness assuming conventional small deflection, zero prestretch beam theory.

The solution to the governing equations is given by

$$\bar{w}(\bar{x}) = \frac{96\bar{P}\left(\Lambda\bar{x} - \sinh\Lambda\bar{x} + (\cosh\Lambda\bar{x} - 1)\tanh\frac{\Lambda}{4}\right)}{\Lambda^3} \tag{5}$$

where the mechanical strain in the beam in the deformed state is given by the solution to

[2]The results are identical for plane strain, provided one substitutes $(1+\nu)\varepsilon_R$ for ε_R and $E/(1-\nu^2)$ for E.

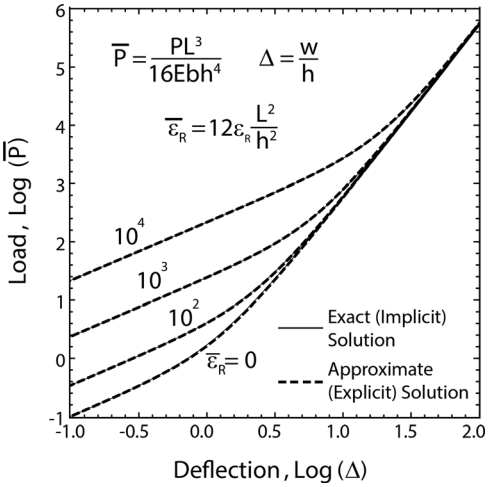

Fig. 1 Exact and approximate load-deflection relationships for a broad range of prestretch

$$\Lambda^2 - \bar{\varepsilon}_R = 12\Delta^2\cdot F(\Lambda) \tag{6}$$

where $\Delta = \bar{w}(1/2)$ is the deflection of the load point, and

$$F(\Lambda) = \frac{\Lambda\left(\text{sech}\frac{\Lambda}{4}\right)^2\left(2\Lambda + \Lambda\cosh\frac{\Lambda}{2} - 6\sinh\frac{\Lambda}{2}\right)}{\left(\Lambda - 4\tanh\frac{\Lambda}{4}\right)^2} \tag{7}$$

The above reflects in implicit load-deflection solution, with Λ determined via the root of Eq. (6). That is, the load-deflection response can be predicted parametrically in terms of the mechanical strain in the beam Λ and prestrain $\bar{\varepsilon}_R$ using Eq. (6) to calculate $\Delta(\Lambda, \bar{\varepsilon}_R)$ and the load $\bar{P}(\Lambda, \varepsilon_R)$ expressed as

$$\bar{P} = \frac{\Lambda^3}{48\left(\Lambda - 4\tanh\frac{\Lambda}{4}\right)}\Delta \tag{8}$$

That is, for a given level of mechanical strain in the beam (Λ) and prestrain ($\bar{\varepsilon}_R$), one can predict the associated deflection using Eq. (6) and the corresponding load using Eq. (8) Examples of the resulting load-deflection relationships are shown in Fig. 1 for several values of normalized prestrain.

An approximate and *explicit* expression for the load-deflection curve, i.e., $\bar{P}(\Delta)$ can be obtained by recognizing that $F(\Lambda)$ is a weak function of Λ across the entire range of possible values, falling from $F(0) = 12/5$ to $F(\infty) = 2$. This is illustrated in Fig. 2(*a*); assuming that $F(\Lambda)$ is a constant, c, leads to the approximation that $\Lambda^2 = \sqrt{12c\Delta^2 + \bar{\varepsilon}_R}$. Using this approximation in Eq. (8), one obtains an explicit relationship for $\bar{P}(\Delta, \bar{\varepsilon}_R)$

$$\bar{P} = \frac{\Delta(12c\Delta + \bar{\varepsilon}_R)^{3/2}}{48\left(\sqrt{12c\Delta^2 + \bar{\varepsilon}_R} - 4\tanh\frac{\sqrt{12c\Delta^2 + \bar{\varepsilon}_R}}{4}\right)} \tag{9}$$

Adopting $c = 2.12$ as an approximation, one obtains a load prediction for a given level of deflection that is within 6% of the exact solution: A plot of the error in predicted load as a function of applied deflection is shown in Fig. 2(*b*) for several values of normalized prestrain $\bar{\varepsilon}_R$. This expression allows for trivial determination of the modulus and prestrain from a load-deflection

measurement, by least squares fitting of the above nonlinear but explicit expression. For completeness, the approximate load-deflection curve is superimposed on the exact solution in Fig. 1: As expected from the less than 6% error over the entire range, the differences appear negligible.

It should be noted that the exact solution (and, hence, the approximate form) assumes moderate rotations, which invokes $\sin w' \approx w'$. This approximation has less than 5% error for $w' \lesssim 0.53(30\,\text{deg})$. The consistency check to ensure moderate rotations is, therefore, given by

$$\frac{4\Delta\sqrt{12c\Delta^2+\bar{\varepsilon}_R}\left(\operatorname{sech}\left[\frac{1}{4}\sqrt{12c\Delta^2+\bar{\varepsilon}_R}\right]-1\right)}{\sqrt{12c\Delta^2+\bar{\varepsilon}_R}-4\tanh\left[\frac{1}{4}\sqrt{12c\Delta^2+\bar{\varepsilon}_R}\right]} \leq \frac{L}{h} \tag{10}$$

This limit on validity will be reached in most cases when $12c\Delta^2 \gg \bar{\varepsilon}_R$, in which case it is simply $w(L/2) < L/4$, i.e., the deflection of the center must be smaller than one-fourth the beam length; otherwise, rotations will not be moderate. This simply states that if the deflection shape is an inverted "V", the angle of the deformed shape must be less than 30 deg.

3 Asymptotic Limits

The approximate solution clearly illustrates that linear load-deflection response is observed when $\bar{\varepsilon}_R \gg 12c\Delta^2$, i.e., in the limit of small deflections. The response in this scenario is given by

$$\bar{P} = \frac{\bar{\varepsilon}_R^{3/2}}{48\left(\sqrt{\bar{\varepsilon}_R}-4\tanh\frac{\sqrt{\bar{\varepsilon}_R}}{4}\right)}\cdot\Delta \tag{11}$$

This is exact for small deflections since the choice of c is immaterial upon neglect of the Δ^2 term. For small deflections, the additional deformation due to the applied load is negligible in comparison to the prestrain $\bar{\varepsilon}_R$. Critically, it should be noted that this limit captures both bending and membrane stretching: The stiffness of the beam is a function of both the bending stiffness and the prestrain in the beam.

The role of prestrain in altering the stiffness of the beam for small deflections can be seen more clearly as follows. The prefactor to Δ in Eq. (11) that depends on $\bar{\varepsilon}_R$ represents the increase in stiffness in the linear regime due to residual stress in the beam. This prefactor is equal to $1+\bar{\varepsilon}_R/40$ in the limit $\bar{\varepsilon}_R \to 0$ and $\bar{\varepsilon}_R/48$ in the limit $\bar{\varepsilon}_R \to \infty$. In the lower limit, bending stiffness still makes a significant contribution to stiffness, while in the upper limit, the stiffness of the beam is entirely due to prestretch.

Approximating the prefactor in Eq. (11) with $1+\bar{\varepsilon}_R/40$ is within 5% of Eq. (11) for $\bar{\varepsilon}_R \leq 337$, which corresponds to scenarios where stiffening due to prestretch is on the same order as the bending stiffness. The upper asymptotic limit (i.e., assuming the prefactor is $\bar{\varepsilon}_R/48$) is within 5% of the full solution for $\bar{\varepsilon}_R \geq 6400$, which simply implies the stiffness increase due to prestretch dominates contributions due to bending stiffness. Assuming residual strains on the order of 0.2%, this implies that the stiffness increase of $1+\bar{\varepsilon}_R/40$ is accurate for beams up to $L/h \leq 400$. On the other hand, for $L/h = 400$, the upper limit (where stiffness scales with $\bar{\varepsilon}_R/48$) is only accurate for residual strains greater than 4%. Considering both asymptotes of the correction with respect to $\bar{\varepsilon}_R$, the linear prediction for the stiffness increase (i.e., $1+\bar{\varepsilon}_R/40$) is less than 20% different from Eq. (11) for all values of residual strain.

In the other extreme (i.e., large deflections), the approximate solution clearly indicates that classical membrane theory with $\bar{P} \propto \Delta^3$ results for scenarios where $12c\Delta^2 >> \varepsilon_R$. In the asymptotic limit where the deflections are quite large, the strain in the beam scales with Δ^2 and the exact solution in this limit corresponds to $c = 2$. The approximate solution stated above assumes $c = 2.12$, implying a 6% error in this limit. One can naturally recover an exact expression in the limit of membrane theory using $c = 2$; however, the error in the approximate form for intermediate deflections (see Fig. 2(*b*)) will be larger than 6%, and hence, $c = 2.12$ is used in the following: It produces relatively small errors for all scenarios. Again, it should be noted that for large deflections, one must check the size of the rotations (i.e., $w'(x)$) to ensure the moderate rotation approximation is valid.

4 Design of Experiments

Given the sophistication of modern instrumentation, tests often span multiple response regimes. To guide the design of experiments that corresponding to a specific regime, Fig. 3 shows combinations of loads, displacements, and prestretch where solutions are governed by linear, membrane, and the transition from linear to nonlinear membrane behavior. The transition region, denoted by hatching in the Fig. 3, is represented by Eq. (9). Upon assuming properties of the material being tested, it is possible to choose beam geometries that will position a large portion of the test in a particular regime. For example, if neither modulus nor prestrain are known, it is desirable to test the beam in the mixed region because nonlinear coupling allows for accurate extraction of both properties. This technique will be shown in the experimental study discussed below.

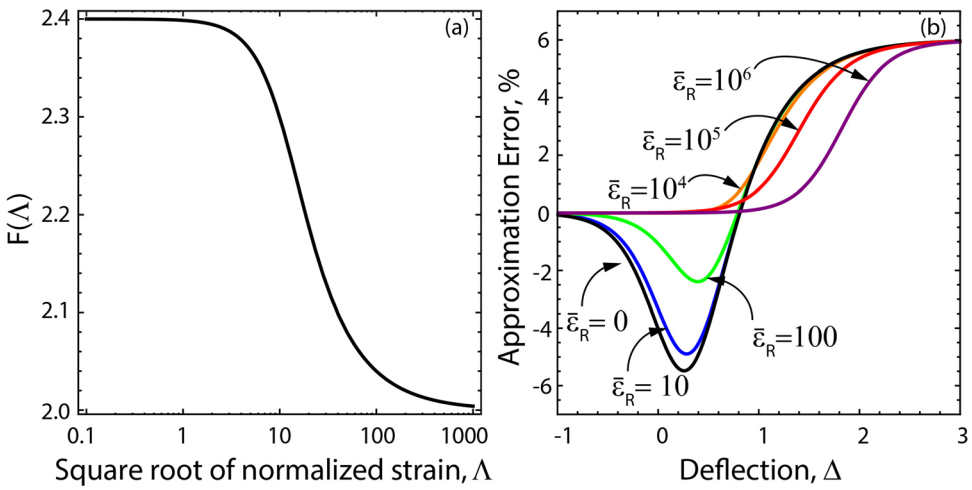

Fig. 2 (*a*) The full range of $F(\Lambda)$ and (*b*) error in the predicted load as a function of applied deflection for values of $\bar{\varepsilon}_R$ from 0–10^6 when $c = 2.12$

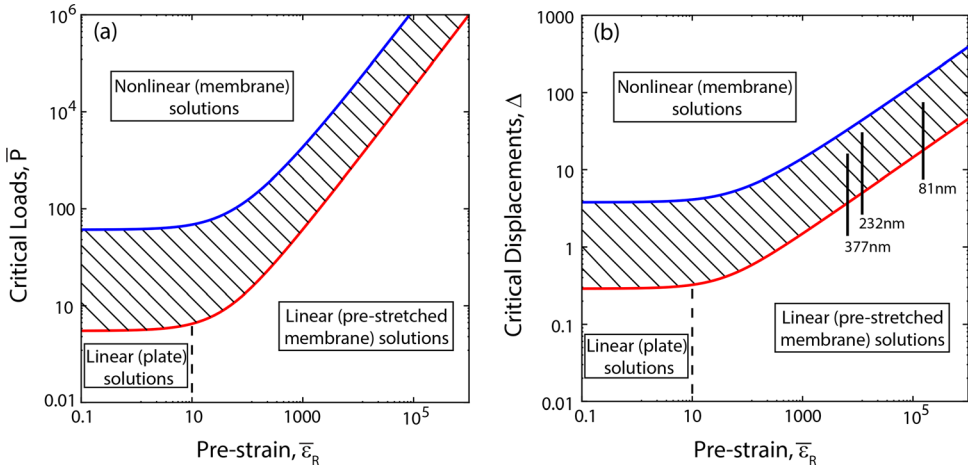

Fig. 3 Illustration of combinations of (*a*) normalized critical loads, (*b*) normalized critical displacements and normalized prestretch for which asymptotic solutions are accurate: the shaded region represents the transition from linear regimes to the membrane regime where the analytical solution can be used to extract material properties. Labeled vertical lines correspond to the range over which experimental data are fit in Sec. 5.

In addition to identifying the relevant type of response in a given scenario, the above analysis also provides insight into values of prestrain and applied deflection where stretching strains dominate bending strains. In some instances, notably the design of tests to explore nonlinear material response, it is desirable to bypass small deflection behavior in favor of the regime associated with pure stretching. While we do not consider nonlinear material response here, the use of the present model is nonetheless informative, as we seek to eliminate the bending regime, which generally corresponds to small strains where elasticity plays a role. The maximum bending strain occurs at the outer skin, i.e., $y = h/2$: One can calculate the bending strain at this location for a given position according to

$$\bar{\varepsilon}_{\text{bending}}(\bar{x}) = \frac{L^2 \varepsilon_{\max}(\bar{x})}{12h^2} = \Lambda^2 + \frac{1}{48}\bar{w}''(\bar{x}) \tag{12}$$

As one would expect, the bending strain is maximum at the clamp and under the point-load (and those two are equal because of symmetry).

Using the approximation that $\Lambda \approx \sqrt{c\Delta^2 + \bar{\varepsilon}_R}$, one obtains the following for the maximum strain in the beam

$$\bar{\varepsilon}_{\max} = \frac{\Delta\sqrt{c\Delta^2 + \bar{\varepsilon}_R}}{24\left(\sqrt{c\Delta^2 + \bar{\varepsilon}_R}\coth\frac{\sqrt{c\Delta^2 + \bar{\varepsilon}_R}}{4}\right) - 96} \tag{13}$$

The above can be used to estimate the deflection that is required to reach yielding at the clamps. The ratio between the contribution due to bending, the last term, and the total strain is of central interest: For large enough deflection, bending strains are negligible and membrane approximations are valid

$$\frac{\varepsilon_{\text{bending}}}{\varepsilon_{\text{total}}} = \frac{\Delta}{\Delta + 24\left(\sqrt{c\Delta^2 + \bar{\varepsilon}_R}\coth\frac{\sqrt{c\Delta^2 + \bar{\varepsilon}_R}}{4}\right) - 96} \tag{14}$$

Though not immediately obvious, the strain ratio given above asymptotes to unity when $\Delta \to 0$, as expected in the small-deflection, pure bending limit. Figure 4 illustrates critical values of residual strain and applied displacement where bending strains contribute a given percentage of the total strain, again assuming

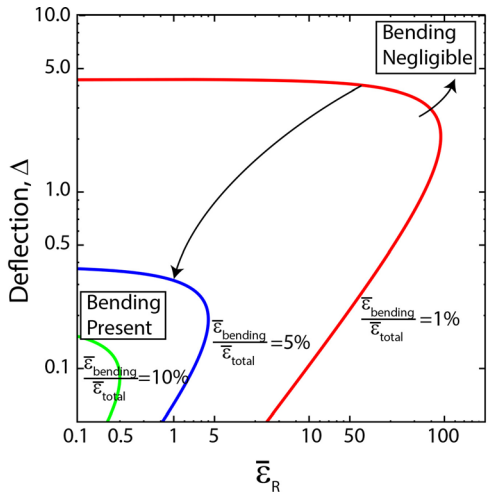

Fig. 4 Contours showing combinations of prestrain and deflections where the contribution of bending strain to the total strain in the beam is 1, 5, and 10%. For applied displacements greater than approximately five times the film thickness bending strains are negligible regardless the level of prestrain.

$c = 2.12$. The results illustrate that pure stretching is obtained for nearly all values of applied displacements (even small ones) when the residual strain is large, as one expects. It is interesting to note that for all values of residual strain bending contributes less than 1% of the total strain for $\Delta > 5$. This is probably an upper limit for the required displacement because yielding at the clamps and load point causes plastic hinges to form, such that bending is further reduced.

5 Illustration: Testing of Nickel Beams

Beams were fabricated on 51 mm (2 in.) *p*-type 100-oriented silicon, which acts as the substrate as well as the sacrificial layer. Prior to depositing the beam film, a bilayer photoresist film (lift-off resist LOR10B and positive photoresist AZ4210) is spun on and patterned, which produces a controlled degree of undercut on the bottom layer, preventing irregularities at the bridge edges after the lift-off process. A titanium adhesion layer was first deposited followed by the nickel beam layer. The nickel (99.995% pure)

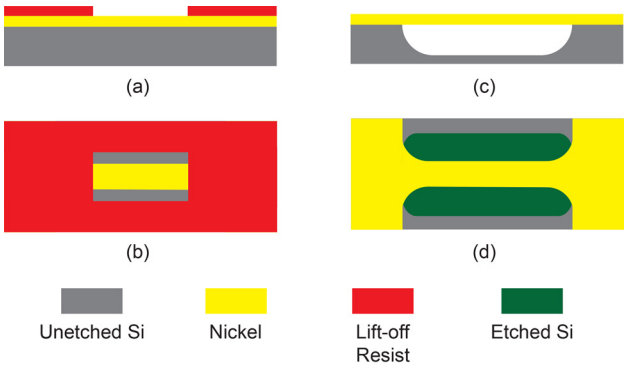

Fig. 5 Illustration of fabrication method for freestanding nickel beams. (*a*) Side and (*b*) top view of beam and photoresist mask prior to silicon etch. (*c*) Side and (*d*) top view postetch and lift off resist removal.

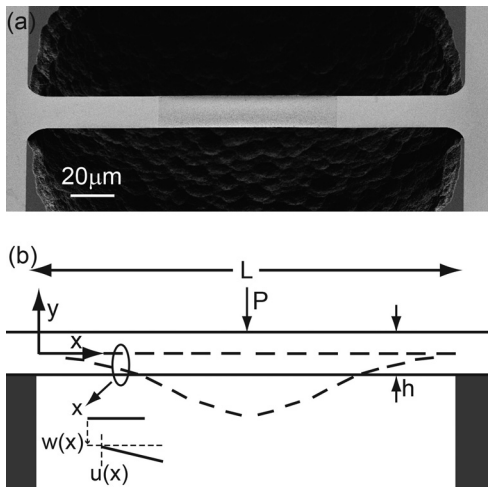

Fig. 6 (*a*) SEM of representative MEMS beam used in point-load test. (*b*) Side view of coordinates and deformation variables used in the analysis.

beams were deposited via electron beam evaporation with a base pressure of 9×10^{-7}. Deposition rates were 0.1 nm/s and 0.2 nm/s for titanium and nickel, respectively. In order to minimize thermal effects on the beams after deposition, lift-off was performed in room temperature *n*-methyl-2-pyrrolidone(NMP) with the help of a low power ultrasonic bath. Film thickness and width were determined with a Veeco Dektak 8 mechanical profiler following calibration on a 48 nm standard and a Wyko NT1100 optical profiler. The standard deviation in thickness and width are ± 1 nm and ± 100 nm.

To define the etch area a second bilayer photoresist film, identical to the first described above, was patterned as shown in Figs. 5(*a*) and 5(*b*). After development the top layer, AZ4210, was removed with acetone leaving the LOR10B. During the evolution of this fabrication procedure we determined that AZ4210 hardens during the etch phase and became too difficult to remove without a high temperature NMP bath, which destroyed the beams. The silicon and titanium layer beneath the beam were removed using an *Xetch*® e1 etcher by cycling 2 mTorr of XeF_2 gas into the etching chamber. The beams were inspected via optical microscopy after three etch phases and then every phase thereafter to determine when the etch was complete. Beams were stopped before overetching occurred so the length of the beam could be determined. The LOR10B layer was removed after etching in a KOH-based developer, AZ400K. The beam length was determined via scanning electron microscopy and optical profilometry resulting in a standard deviation of ± 0.5 μm. Energy dispersive X-ray spectroscopy (EDX) on the underside of beams confirmed the titanium is removed during the etch. Figure 6(*a*) and Figs. 5(*c*) and 5(*d*) show a beam postrelease. The trench under the beams is on the order of ~ 60 μm, which allows for large deflections without etching from the backside of the wafer.

The released beams were probed in the center of e span using a *NanoIndenter*® DCM (Agilent Technologies, Chandler, AZ) equipped with a 50 μm radius sapphire sphere. It is very unlikely that off-axis loading is a concern in the present tests or those conducted with similar hardware. The precision of the positioning of the indenter head (i.e., several microns), the indenter tip radius and the beam widths are such that complete contact across the width of the beam is ensured. Further, small amounts of twist are unlikely to have much of an effect in the membrane limit because the vast majority of the beam is stretched uniformly: Bending effects are confined to a narrow region near the clamp and the load point should off-axis effects be present. Tests were performed using a method that determines the instant of contact by observing changes in a small harmonic oscillatory load superimposed over the approach ramp load [22,23]. By identifying the instant where the harmonic displacement drops (or increases depending on operating frequency) by an amount greater than the environmental noise, which is usually less than 1 nm [4,22], the position of the probe at the instant of contact can be determined to within several nanometers. Using this method allows for testing of low stiffness structures on the order of 1 N m^{-1}. In addition to load displacement data, many indentation systems provide direct measurement of stiffness. Although not explicitly addressed here, the small displacement asymptotic limits presented above can be

Table 1 Experimental results

Dimensions (μm) (length, width, thickness)	E (GPa)	$\bar{\varepsilon}_R$	ε_R	R^2
193, 20.97, 0.081	172.3	87,007	0.00128	0.999
193, 20.97, 0.081	180.9	104,672	0.00153	0.999
192, 20.97, 0.081	172.1	108,974	0.00162	0.999
	175.1 ± 5	100,218 ± 11641	0.001474 ± 0.000176	
188, 20.68, 0.232	174.7	13,467	0.00171	0.999
187, 20.68, 0.232	172.7	13,270	0.0017	0.999
189, 20.68, 0.232	182.1	10,294	0.001293	0.999
	176.5 ± 5	12,344 ± 1778	0.001568 ± 0.000239	
200, 20.63, 0.377	174.1	6830	0.002022	0.999
200, 20.63, 0.377	180.3	5534	0.001639	0.999
200, 20.63, 0.377	184.9	6148	0.00182	0.999
	179.8 ± 5.4	6171 ± 648	0.001827 ± 0.000192	

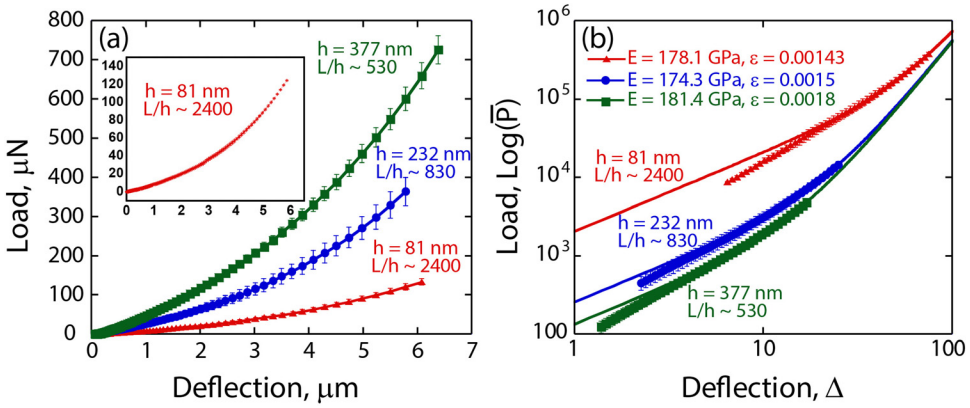

Fig. 7 Raw (*a*) and normalized (*b*) load-displacement curves. The inset graph in (*a*) shows the load and unload curve for the average of six tests on a single 81 nm thick beam showing repeatable results and negligible thermal drift over the duration of the test. Error bars in (*a*) and (*b*) are the average of tests on three different beams for each film thickness. Data shown is below 0.2% to ensure elastic behavior. In (*b*) data below 500 nm are truncated to ensure the beam and indenter are in full contact.

used with stiffness measurements in small displacement regimes where load is proportional to displacement.

Three different beams with nominal length 200 μm and width 20 μm were tested for films with thickness 81, 232, and 377 nm. The measured dimensions for these beams are in the first column of Table 1. Figure 7 shows experimental data and theoretical fits to Eq. (9), with $c = 2.12$, for the average of tests on three beams within each thickness. For very small deflections/loads, the data fall below the predictions (an effect dramatized by the use of a log scale to illustrate small numbers), due to the fact that contact across the width of the beam is not established until larger deflections.

In order to examine the effects of thermal drift on load-displacement behavior, a series of six tests on a single 81 nm thick beam was performed over 120 s as shown in the inset of Fig. 7(*a*). All tests were performed after the system settled to a drift of $<0.05\,\text{nm/s}^{-1}$. The load and unload curves show nearly identical behavior. The small load offset of 490 nN at the completion of the tests in the inset of Fig. 7 is directly attributed to drift in the system. Although this offset can be accounted for in data processing it is not necessary as it accounts for less than 0.5% of the maximum load seen during the test.

Results in Table 1 show the individual tests and results from a least-squares fit to Eq. (9), with $c = 2.12$. Note that the least-squares fit deemphasizes the role of the data at small deflections, i.e., that shown in Fig. 7, that falls beneath the theoretical predictions. The results of these tests and the use of Eq. (9) are extremely consistent from beam to beam (despite variations in dimension), and entirely consistent with work performed on prior nickel thin films. Modulus has been shown to vary from 100–205 GPa with most tests falling in the 160–200 GPa range [24–27].

6 Concluding Remarks

The exact and approximate solutions presented in this paper represent a complete framework that describes the effects of film geometry, prestrain, elastic properties, loads, and displacements on the mechanical response of freestanding point loaded beams. A pair of design maps displays loads, displacements, and prestrains designating when linear, nonlinear membrane, or approximate solutions can be used to extract material properties. These design maps can be used a priori to identify geometric properties that will allow experiments to span particular or multiple testing regimes. Experimental results are presented on nickel beams using the approximate solution showing good agreement with properties found in literature for nickel thin films.

References

[1] Zhang, T.-Y., Su, Y.-J., Qian, C.-F., Zhao, M.-H., and Chen, L.-Q., 2000, "Microbridge Testing of Silicon Nitride Thin Films Deposited on Silicon Wafers," Acta Mater., **48**(11), pp. 2843–2857.

[2] Espinosa, H., Prorok, B., and Fischer, M., 2003, "A Methodology for Determining Mechanical Properties of Freestanding Thin Films and MEMS Materials," J. Mech. Phys. Solid., **51**(1), pp. 47–67.

[3] Wang, L., and Prorok, B., 2007, "Characterization of the Strain Rate Dependent Behavior of Nanocrystalline Gold Films," J. Mater. Res., **23**, pp. 55–65.

[4] Herbert, E., Oliver, W., De Boer, M., and Pharr, G., 2009, "Measuring the Elastic Modulus and Residual Stress of Freestanding Thin Films Using Nanoindentation Techniques," J. Mater. Res., **24**(9), pp. 2974–2985.

[5] Denhoff, M. W., 2003, "A Measurement of Young's Modulus and Residual Stress in MEMS Bridges Using a Surface Profiler," J. Micromech. Microeng., **13**(5), pp. 686–692.

[6] Mulloni, V., Colpo, S., Faes, A., and Margesin, B., 2013, "A Simple Analytical Method for Residual Stress Measurement on Suspended MEM Structures Using Surface Profilometry," J. Micromech. Microeng., **23**(2), p. 025025.

[7] Heidelberg, A., Ngo, L. T., Wu, B., Phillips, M. A., Sharma, S., Kamins, T. I., Sader, J. E., and Boland, J. J., 2006, "A Generalized Description of the Elastic Properties of Nanowires," Nano Lett., **6**(6), pp. 1101–1106.

[8] Ngo, L. T., Almécija, D., Sader, J. E., Daly, B., Petkov, N., Holmes, J. D., Erts, D., and Boland, J. J., 2006, "Ultimate Strength Germanium Nanowires," Nano Lett., **6**(12), pp. 2964–2968.

[9] Wang, Z.-J., Liu, C., Li, Z., and Zhang, T.-Y., 2010, "Size Dependent Elastic Properties of Au Nanowires Under Bending and Tension—Surfaces Versus Core Nonlinearity," J. Appl. Phys., **108**(8), p. 083506.

[10] Zeng, D., and Zheng, Q., 2010, "Large Deflection Theory of Nanobeams," Acta Mech. Solid. Sin., **23**(5), pp. 394–399.

[11] Celik, E., Guven, I., and Madenci, E., 2011, "Mechanical Characterization of Nickel Nanowires by Using a Customized Atomic Force Microscope," Nanotechnology, **22**(15), p. 155702.

[12] Wang, X., Najem, J. F., Wong, S.-C., and Tak Wan, K., 2012, "A Nano-Cheese-Cutter to Directly Measure Interfacial Adhesion of Freestanding Nano-Fibers," J. Appl. Phys., **111**(2), p. 024315.

[13] Zhan, H., and Gu, Y., 2012, "Modified Beam Theories for Nanowires Considering Surface/Intrinsic Effects and Axial Extension Effect," J. Appl. Phys., **111**(8), p. 084305.

[14] Seker, E., Gaskins, J. T., Bart-Smith, H., Zhu, J., Reed, M. L., Zangari, G., Kelly, R., and Begley, M. R., 2007, "The Effects of Post-Fabrication Annealing on the Mechanical Properties of Freestanding Nanoporous Gold Structures," Acta Mater., **55**(14), pp. 4593–4602.

[15] Seker, E., Gaskins, J. T., Bart-Smith, H., Zhu, J., Reed, M. L., Zangari, G., Kelly, R., and Begley, M. R., 2008, "The Effects of Annealing Prior to Dealloying on the Mechanical Properties of Nanoporous Gold Microbeams," Acta Mater., **56**(3), pp. 324–332.

[16] Djalali, R., Chen, Y.-F., and Matsui, H., 2002, "Au Nanowire Fabrication From Sequenced Histidine-Rich Peptide," J. Amer. Chem. Soc., **124**(46), pp. 13660–13661.

[17] Xiao, Z., Han, C. Y., Welp, U., Wang, H., Kwok, W., Willing, G., Hiller, J., Cook, R., Miller, D., and Crabtree, G., 2002, "Fabrication of Alumina Nanotubes and Nanowires by Etching Porous Alumina Membranes," Nano Lett., **2**(11), pp. 1293–1297.

[18] Simmonds, J., Begley, M., and Komaragiri, U., 2005, "The Mechanical Response of Freestanding Circular Elastic Films Under Point and Pressure Loads," ASME J. Appl. Mech., **72**(2), pp. 203–212.

[19] Landau, L. D., and Lifshitz, E., 1970, *Theory of Elasticity*, Pergamon, Oxford.
[20] Senturia, S., D., 2001, *Microsystem Design*, Kluwer Academic Publishers, Norwell, MA.
[21] Espinosa, H., Zhu, Y., Fischer, M., and Hutchinson, J., 2003, "An Experimental/Computational Approach to Identify Moduli and Residual Stress in MEMS Radio-Frequency Switches," Exper. Mech., **43**(3), pp. 309–316.
[22] Oliver, W. C., and Pharr, G., 1992, "An Improved Technique for Determining Hardness and Elastic Modulus Using Load and Displacement Sensing Indentation Experiments," J. Mater. Res., **7**(6), pp. 1564–1583.
[23] Maner, K. C., Begley, M. R., and Oliver, W. C., 2004, "Nanomechanical Testing of Circular Freestanding Polymer Films With Sub-Micron Thickness," Acta Mater., **52**(19), pp. 5451–5460.
[24] Luo, J., Flewitt, A., Spearing, S., Fleck, N., and Milne, W., 2004, "Young's Modulus of Electroplated Ni Thin Film for MEMS Applications," Mater. Lett., **58**(17), pp. 2306–2309.
[25] He, S., Chang, J. S., Li, L., and Ho, H., 2009, "Characterization of Young's Modulus and Residual Stress Gradient of MetalMUMPs Electroplated Nickel Film," Sensor. Actuat. A: Physical, **154**(1), pp. 149–156.
[26] Majjad, H., Basrour, S., Delobelle, P., and Schmidt, M., 1999, "Dynamic Determination of Young's Modulus of Electroplated Nickel Used in LIGA Technique," Sensor. Actuat. A: Physical, **74**(1), pp. 148–151.
[27] Namazu, T., and Inoue, S., 2007, "Characterization of Single Crystal Silicon and Electroplated Nickel Films by Uniaxial Tensile Test With In Situ X-Ray Diffraction Measurement," Fatique Fract. Eng. Mat. Struct., **30**(1), pp. 13–20.